Inelastic-electron-scattering cross sections for Si, Cu, Ag, Au, Ti, Fe, and Pd

S. Tougaard and J. Kraaer
Fysisk Institut, Odense Universitet, DK-5230 Odense M, Denmark
(Received 2 July 1990)

Inelastic-scattering cross sections of 300–10 000-eV electrons in Si, Ti, Fe, and Pd and of 300–2000-eV electrons in Cu, Ag, and Au have been investigated theoretically and experimentally. The product of the inelastic mean free path and the cross section were determined experimentally through an analysis, based on a recent formula, of reflection electron-energy-loss spectra. To study energies above 2000 eV a special experimental setup was developed. Theoretical cross sections were determined through a dielectric-response description of the solid-electron interaction using Drude-Lindhard model dielectric functions. At high energies, good agreement is observed between theoretically and experimentally determined cross sections. At lower energies differences are observed. These are discussed partly in terms of a breakdown of the dielectric model used, and partly surface excitations.

I. INTRODUCTION

The inelastic-scattering properties of high-energy (≥ 10 keV) electrons in solids have been studied extensively in the past.[1–3] In contrast, very limited quantitative information is available on the cross section of low-energy (≤ 10 keV) electrons in solids.

This energy range is particularly important since the widely used surface electron spectroscopies, x-ray photoelectron spectroscopy (XPS), Auger electron spectroscopy (AES), and reflection electron-energy-loss spectroscopy (REELS) rely on analysis of the energy distribution of emitted low-energy electrons. Due to inelastic scattering, surface electron spectra are distorted during electron transport out of the solid and a correction is necessary before any quantitative spectral analysis can be performed.[4] To correct for this, detailed knowledge on the inelastic cross section is essential.[5,6] Besides, inelastic-scattering cross sections are essential in the evaluation of electron slowing down and of damage produced by energetic electrons in solids.

There are both experimental and theoretical reasons for the lack of investigations on this topic. Theoretical model calculations rely on a dielectric-response description of the solid-electron interaction.[7–11] The problem here is that the complex dielectric-response function of the particular solid must be known in detail with respect both to energy and to momentum transfers. In general, such information is not available. Methods based on model dielectric functions have been developed[8] and applied to various solids.[9–11] For low-energy electrons, the validity of these models is, however, hard to establish solely on theoretical grounds. Therefore it is of high interest to be able to test such cross sections experimentally.

Experimental cross sections for high-energy electrons have been successfully studied by analysis of the energy distribution of a monoenergetic beam of electrons after traversing a thin slab of the solid.[1] For these experiments to be sensitive, the slab thickness should be less than a few times the mean free path λ for inelastic electron scattering. λ decreases for decreasing electron energy and typical values for energies of 2000 and 300 eV are $\lambda \cong 20-40$ Å and $\lambda \cong 6-10$ Å, respectively.[12,13] For electron energies below a few thousand electron volts, extremely thin samples are therefore needed and this type of experiment is, because of obvious experimental difficulties, not applicable.

Recently, it was shown that quantitative differential cross-section information can be obtained through proper analysis of REELS spectra.[14] The approach was applied to aluminum. Being a free-electron-like metal, structure corresponding to multiple plasmon excitations can clearly be observed. Aluminum therefore served as a perfect basis for a test of the validity of the method, since the origin of different structures in the cross section could easily be identified.[14]

To gain more insight into the inelastic-scattering properties of solids and to find the limits of validity of the theoretical approach, it was then decided to initiate a systematic investigation of cross sections for a broad range of solids. Thus, in the present paper, we report on experimental cross sections for Si, Cu, Ag, Au, Ti, Fe, and Pd determined through analysis of experimental REELS spectra for primary electron energies in the 300–10 000-eV range. Theoretical cross sections evaluated on the basis of Drude-Lindhard model dielectric-response functions are also reported. Finally the two sets of cross sections are compared and possible explanations for observed deviations are discussed.

II. THEORY

A. Inelastic-scattering cross sections from REELS

Let a beam of electrons of energy E_0 be incident on the sample surface and let $j_l(E)$ be the measured energy distribution of backreflected electrons. Now, assume that

the sample is a homogeneous medium in the sense that as the electron travels in the solid, the probability $K(E_0,T)$ for energy loss T per unit path length and per unit energy loss is a constant function of T, independent of the actual depth underneath the solid surface. Then[14]

$$\frac{\lambda L}{\lambda+L}K(E_0,E_0-E) = \frac{j_l(E)-\int_E^{E_0}\frac{\lambda L}{\lambda+L}K(E_0,E'-E)j_l(E')dE'}{\int_{E_0^-}^{E_0^+}j_l(E')dE'} , \quad (1)$$

where L is the characteristic length for the distribution of path lengths experienced by the electrons prior to emission. Based on a $P1$ approximation to the Boltzmann transport equation, it was found that $L\cong 2\lambda_1$ where λ_1 is the transport mean free path for elastic electron scattering.[15] Since the cross section for elastic electron scattering is strongly peaked in the forward direction, we have in general $\lambda_1>\lambda$, then $L\gg\lambda$, and

$$\frac{\lambda L}{\lambda+L}\cong\lambda . \quad (2)$$

For a numerical treatment, the REELS spectrum is divided into channels E_i of width ΔE. We take $i=0$ at E_0 and increasing integers i for increasing energy loss and get from Eqs. (1) and (2)

$$\lambda(E_0)K(E_0,E_0-E_i) = \left[j_l(E_i)-\sum_{m=1}^{i-1}\lambda(E_0)K(E_0,E_m-E_i)j_l(E_m)\Delta E\right] \times\frac{1}{j_l(E_0)\Delta E} , \quad (3)$$

where $j_l(E_0)\Delta E$ is the integrated intensity in the elastic-scattering peak.

In practice, the elastic peak may be separated from the inelastic part of the spectrum by first locating the minimum intensity point on the low-energy side of the elastic peak. Then a straight line is drawn from this point to zero intensity at the primary energy E_0. This defines the inelastic spectrum $j_l(E)$ for $E\le E_0$ and $j_l(E_0)\Delta E$ is the area between the peak and the straight line. This procedure is arbitrary, and as a result, the loss spectrum and thereby the determined $\lambda K(T)$ is not well known for energy loss $\le 1-2$ eV.

Note that the intensities in the elastic and inelastic parts of the REELS spectra differ by a factor of up to ~ 100. Due to this large dynamic range, it is of paramount importance to check that the analyzer operates linearly. If the system is equipped with an x-ray facility, the analyzer linearity can be checked by measuring the same XPS peak with two widely different x-ray emissions but otherwise identical experimental settings. For the analyzer to operate linearly, the shape of these two spectra must be identical. As an alternative linearity test, two REELS spectra are measured, one with the primary beam current normally used and one with a factor of 5–10 lower primary beam current. For the two spectra, the ratio of the elastic peak area to the inelastic background, e.g., 30 eV from the peak energy must then be identical for the system to operate linearly. (Note that the peak area and not the peak height should be used in this test, since the width of the primary peak varies with the beam current.) If the analyzer is found to respond nonlinearly, the primary beam current may have to be lowered, and/or the multiplier voltage may have to be increased.

This linearity requirement sets a limit on the maximum beam current that can be used. To decrease the total time needed to produce a spectrum, with a given signal-to-noise ratio, it may therefore be taken in two steps. The first spectrum is measured in a limited energy range around the elastic peak (e.g., E_0-20 eV $<E<E_0+5$ eV) with a low primary beam current to assure linearity and a fine energy grid (e.g., 0.05 eV) (to get a good definition of the sharp elastic peak). The second spectrum is recorded in the energy range $E<E_0-3$ eV with a higher beam current (because the maximum spectral intensity is much lower in this energy range) and with a slightly larger energy grid (e.g., 0.1 eV). Then the second spectrum is normalized to the first spectrum by the ratio of the areas of the two spectra in the energy interval E_0-20 eV to E_0-5 eV. Finally, the energy grid in the second spectrum is increased, by simple interpolation, to match the energy grid of the first spectrum and from the two spectra a single spectrum is produced which includes the elastic peak and the full energy-loss spectrum.

If the elastic peak is not measured, Eq. (3) may still be used with $j_l(E_0)\Delta E$ as an adjustable parameter. One can then, for example, use the criterion that $\lambda(E_0)K(E_0,E_0-E_i)\simeq 0$ for $E_0-E_i\ge 150$ eV.

Equation (3) is a recursion formula in the sense that to evaluate $\lambda K(E_0,T)$ for a given value of T, the range of $\lambda K(E_0,E_m-E_i)$ values needed on the right-hand side of Eq. (3) is limited to $E_m-E_i<T$. To evaluate $\lambda K(E_0,T)$, one then starts with $T=0$ [since $K(T=0)=0$] and successively evaluates for all values of T.[5,14]

B. Inelastic-scattering cross sections from model dielectric functions

According to the work by Lindhard,[7] the probability that an electron of energy E shall lose energy $\hbar\omega$ per unit energy loss and per unit path length traveled in the solid is

$$K(E,\hbar\omega)=\frac{1}{\pi E a_0}\int_{k^-}^{k^+}dk\frac{1}{k}\mathrm{Im}\left[-\frac{1}{\epsilon(k,\omega)}\right] , \quad (4)$$

where $k^{\pm}=(2m/\hbar^2)^{1/2}(\sqrt{E}\pm\sqrt{E-\hbar\omega})$ and a_0 is the Bohr radius. $\epsilon(k,\omega)$ is the complex dielectric function, which describes the response of the solid to the moving electron in terms of energy and momentum transfers to the electrons of the solid.

As a model for the dielectric loss function, we follow previous work[8] and expand in terms of Drude-Lindhard functions

$$\mathrm{Im}\left[-\frac{1}{\epsilon(k,\omega)}\right] = \sum_i \frac{A_i \gamma_i \hbar\omega}{\left[\left(\hbar\omega_{0i}+\frac{\hbar^2k^2}{2m}\right)^2-\hbar^2\omega^2\right]^2+(\gamma_i\hbar\omega)^2} . \quad (5)$$

For $k \to 0$, the optical limit is approached, and the expansion coefficients may be determined from a fit of Eq. (5) to $\mathrm{Im}[-1/\varepsilon(0,\omega)]$ as determined from optical or from high-energy thin-film electron transmission experiments.

The dependence of $\epsilon(k,\omega)$ on k is in general unknown and extrapolations must be made. The choice in Eq. (5) gives the correct limiting value for $k \to \infty$, and also ensures that the dielectric function satisfies certain sum rules for all values of k.[8]

It is not possible on theoretical grounds to establish the accuracy of this model dielectric function. Consequently, experimental tests of cross sections determined by this procedure are highly important.

III. EXPERIMENT

The mechanically polished samples were mounted in a UHV chamber with a base pressure below 10^{-10} Torr. They were cleaned by Ar^+ ion bombardment. All samples were polycrystalline except the Si(111) single crystal which was bombarded with 5-keV Ar^+ ions to destroy the crystallinity of the sample. For Si, Ti, Fe, and Pd the sample was subsequently annealed to a few hundred degrees centigrade to remove implanted Ar. The surface contamination was frequently checked by XPS, and only samples with a surface contamination below 1% with respect to any contamination were considered acceptable.

REELS spectra were measured with a hemispherical electron-energy analyzer (VG-Clam) which operates up to 2000-eV energy. The separation of the spectra in elastic and inelastic parts as well as a careful check on the linearity of the analyzer were performed as described in Sec. II A. The angles from the surface normal to the electron gun and the analyzer are given in Fig. 1. The measured spectra were corrected for the energy dependence of the analyzer transmission function which for this type of analyzer is $\cong E^{1/2}$.[16] Experiments were first performed for Cu, Ag, and Au in the 0–2000-eV energy range and preliminary results for Au were published in Ref. 17. However, discrepancies were found between theoretical and experimental cross sections. It was then decided to do more extensive investigations including a range of solids: Si, Ti, Fe, and Pd. Since one would expect the theoretical cross sections to be most accurate at the high energies (see discussion below), it is of interest to determine experimental cross sections at high energies and gradually go to lower energies. This could give more information on the reasons why the theoretical description breaks down.

The electron-energy analyzer used here only operates for electron energies below 2000 eV. To achieve REELS spectra at higher energies, an experimental device as illustrated in Fig. 1 was designed. It consists of two spherical grids separated by a ceramic ring and a planar grid in electrical contact with the sample. The outer grid is on ground potential, while the inner grid, the planar grid, and the sample are on a common potential U which can be varied. The basic idea is the following: the electrons are accelerated in the region between the spherical grids and continue in the field free space towards the sample. The backreflected electrons move along straight lines towards the analyzer and are decelerated in passing through the region between the two grids. Thus the electron gun and the energy analyzer are both operated at a low energy, while all the physical processes in the sample occur at a higher energy determined by the voltage U and electron gun beam energy.

The spherical grids were shaped from stainless-steel grids by stretching over a stainless-steel ball. After annealing at 750 °C for 3 h and subsequent slow cooling ($\sim$6 h) in the oven, the grids are stable and can be cut, electropolished, and mounted on the sample holder. To minimize the possible error introduced by the experimental setup, the electron gun was always operated at the highest possible analyzer energy, i.e., 2 keV when studying cross sections above 2-keV energy.

The error introduced by the setup in Fig. 1 is determined by the degree of perfection of the spherical grids. Consequently, experimental tests of the performance are important.

Since the critical quantity here is the relative deceleration of the electrons in passing the grid system, the quality of the device was tested by the following procedure. The most critical situation is for a 10-keV primary electron energy at the sample. The electron gun is operated at 2 keV. Then the ratio of the acceleration energy (8 keV) to the electron-beam energy (2 keV) is 4. Therefore

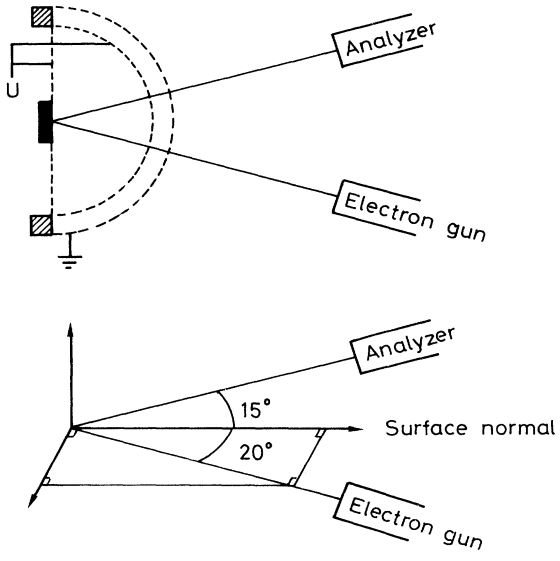

FIG. 1. Upper part: The experimental setup used for measurement of REELS at energies greater than 2 keV. Lower part: The geometry of the experiments.

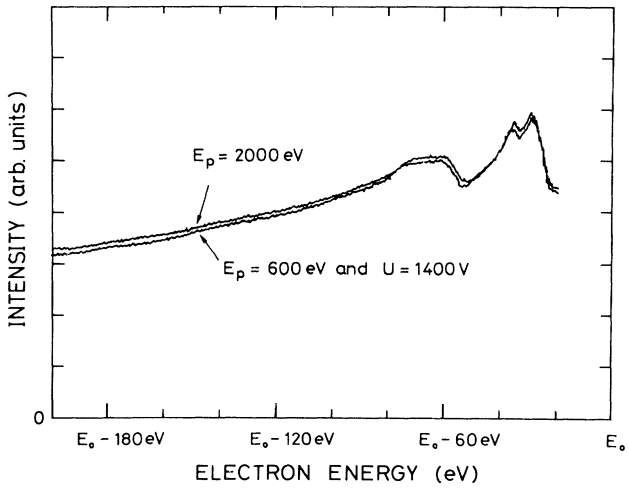

FIG. 2. Test on the performance of the experimental setup in Fig. 1 in the most critical situation.

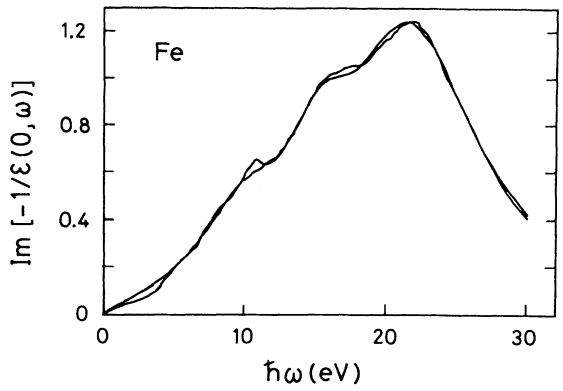

FIG. 3. Fit of the Drude-Lindhard expansion in Eq. (5) and the experimental Im($-1/\epsilon$) data for Fe. Similar fits were made for the other materials studied.

the performance of the analyzer is tested by recording a loss spectrum for an electron gun beam energy $E_p=2$ keV with the grids removed. Next, a spectrum is recorded with the grid system, a primary electron energy of $E_p=600$ eV, and accelerating voltage of 1400 V. The spectra are recorded up to 200-eV energy loss. The ratio of the acceleration energy (1400 eV) to the lowest energetic electron entering the grid system (600–200 eV=400 eV) is $\cong 4$. By comparing these two spectra, we can then judge the performance of the device in the most critical situation.

Figure 2 shows the two spectra for Pd after correction for the energy dependence of the analyzer transmission function. The maximum deviation between the two spectra is 2% for $E_0-E<100$ eV increasing to 4% for $E_0-E\simeq 200$ eV. This test was also performed at other less critical sets of energies and accelerating voltages where even better agreement was found. It is then concluded that the device in Fig. 1 operates with an accuracy better than 2% for primary electron energies up to ~ 10 keV and energy loss up to 100 eV.

IV. RESULTS

A. Theoretical cross sections

Theoretical cross sections were evaluated by the procedure outlined in Sec. II. For Fe and Pd, the function Im$[-1/\epsilon(0,\omega)]$ was taken from optical data,[18] while for Ti, Cu, Ag, and Au it was taken from high-energy thin-

TABLE I. Drude expansion coefficients determined from the best least-squares fit of Eq. (5) to available data for Im($-1/\epsilon$) (see Sec. IV A).

i	$\hbar\omega_{0i}$ (eV)	A_i (eV^2)	γ_i (eV)	$\hbar\omega_{0i}$ (eV)	A_i (eV^2)	γ_i (eV)	$\hbar\omega_{0i}$ (eV)	A_i (eV^2)	γ_i (eV)
		Cu			Ag			Au	
1	4.50	1.10	2.50	3.91	1.40	0.63	3.09	0.27	0.56
2	8.3	5.3	4.0	8.4	10.1	4.2	5.99	2.56	3.18
3	12.8	19.4	6.9	13.3	11.7	8.3	11.8	13.5	7.6
4	21.4	139.1	10.8	17.7	23.8	6.1	16.6	29.7	6.3
5	29.2	34.3	5.4	25.1	73.7	6.8	25.1	84.2	6.6
6	34.8	373.9	32.1	33.0	30.9	5.8	33.2	69.6	6.0
7	65.0	350.0	50.0	49.5	990.9	51.7	45.1	923.7	33.9
8				55.2	17.2	5.5			
9				68.0	50.0	9.9			
10				81.6	462.2	31.1			
		Ti			Fe			Pd	
1	9.5	7.0	5.0	10.8	25	8	7.8	7	2
2	19.9	218	7.0	15.5	26	5	10.5	20	7
3	25.0	40	5	22.5	310	12	16.15	8	3
4	40.0	50	10				27.4	410	15
5	50.0	480	15						
6	90.0	50	20						

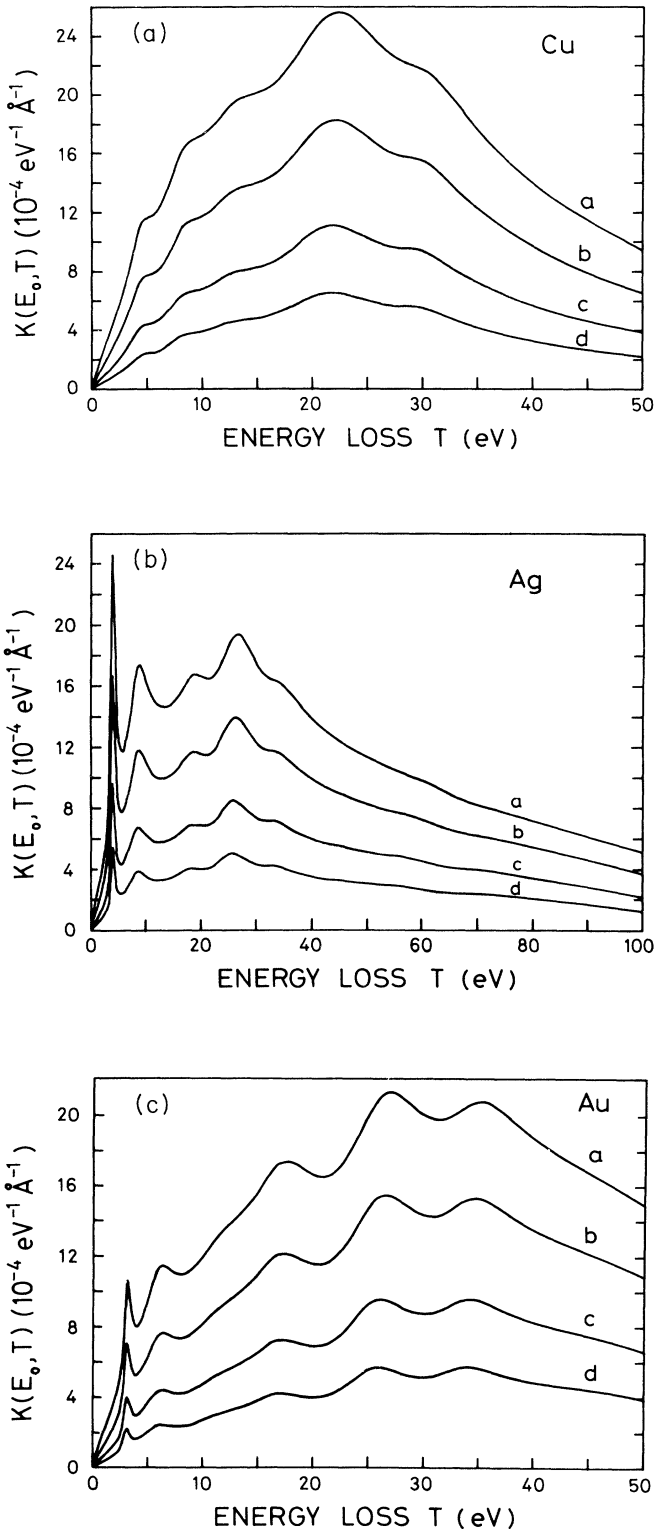

FIG. 4. Theoretical inelastic-electron-scattering cross section for electrons of varying energies in Cu, Ag, and Au evaluated from Eq. (4) and the fit in Eq. (5). Curves *a*, $E_0=300$ eV; curves *b*, $E_0=500$ eV; curves *c*, $E_0=1000$ eV; and curves *d*, $E_0=2000$ eV.

film transmission experiments.[19,20] Three to ten terms were used in the expansion [Eq. (5)], to get a satisfactory fit. The expansion coefficients are listed in Table I. As an example, Fig. 3 shows the loss function and the fit for Fe.

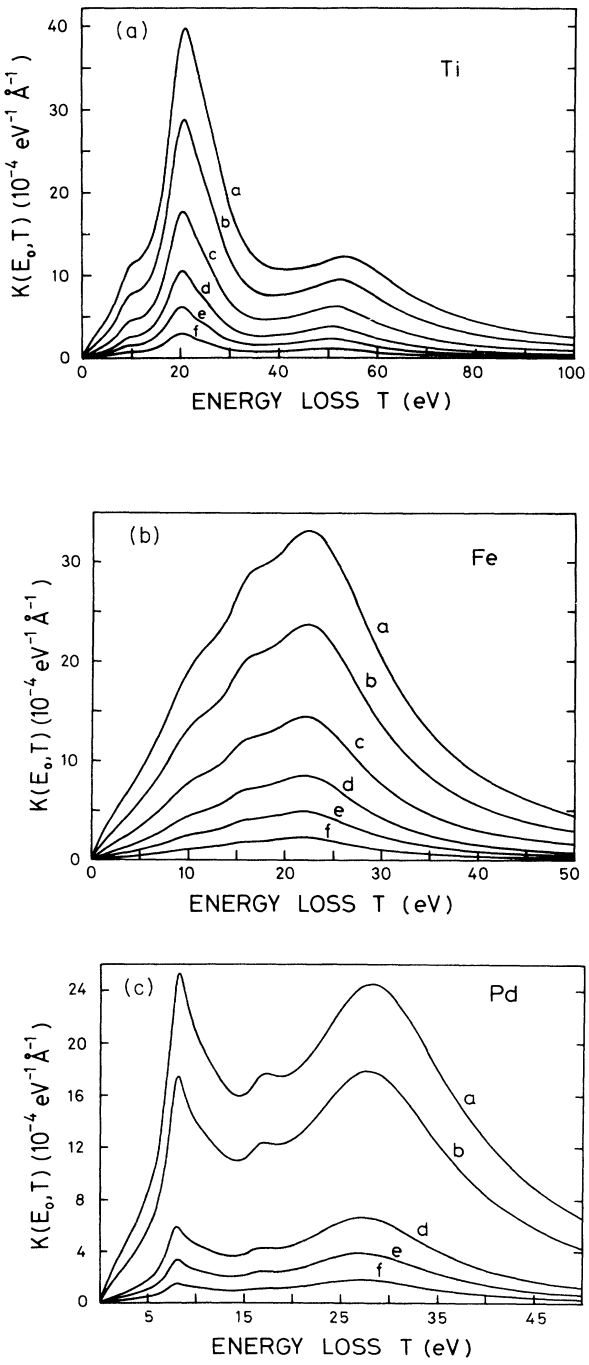

FIG. 5. Theoretical inelastic-electron-scattering cross sections for electrons of varying energies in Ti, Fe, and Pd evaluated from Eq. (4) and the fit in Eq. (5). Curves *a*, $E_0=300$ eV; curves *b*, $E_0=500$ eV; curves *c*, $E_0=1000$ eV; curves *d*, $E_0=2000$ eV; curves *e*, $E_0=4000$ eV; curves *f*, $E_0=10\,000$ eV.

TABLE II. Factors λ in angstroms used for the theoretical curves labeled *t* in Figs. 9–14. Note that only for Ti and Ag are these values believed to be a reasonable approximation for the inelastic mean free path (see the discussion in Sec. IV B).

E_0	0.3 keV	0.5 keV	1 keV	1.5 keV	2 keV	3 keV	6 keV	10 keV
Cu			17.9	25.6	32.3			
Ag	7.6			21.5	28.4			
Au	10.1	16.0	17.6	21.4	26.8			
Ti	7.3	11	20			50	90	138
Fe	8.7	12	24		36	49	90	137
Pd	11.5	13.5		25	32	46	81	125

The fit was made within the energy range available for $\mathrm{Im}(-1/\epsilon)$, i.e., 0–30 eV for Fe and Pd, 0–50 eV for Cu and Au, and 0–100 eV for Ag and Ti.

Now the inelastic-scattering cross sections are readily evaluated numerically by Eq. (4). Figures 4 and 5 show the resulting cross sections for primary electron energies in the 0.3–2-keV energy range for Cu, Ag, and Au and the 0.3–10-keV energy range for Ti, Fe, and Pd.

As the primary energy is increased, the cross-section function in general decreases as one would expect. At the same time, the relative intensity of the different structures changes and peak positions are slightly shifted.

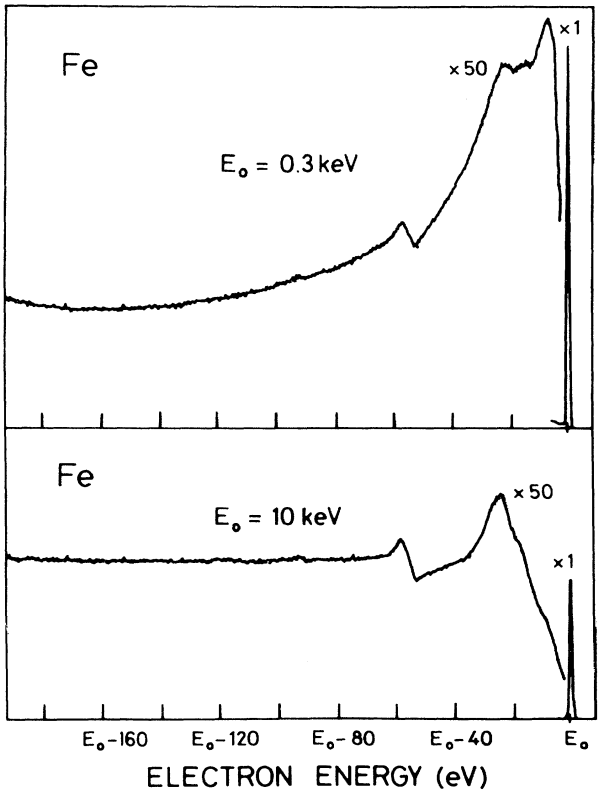

FIG. 6. REELS from Fe at 0.3 and 10 keV, respectively.

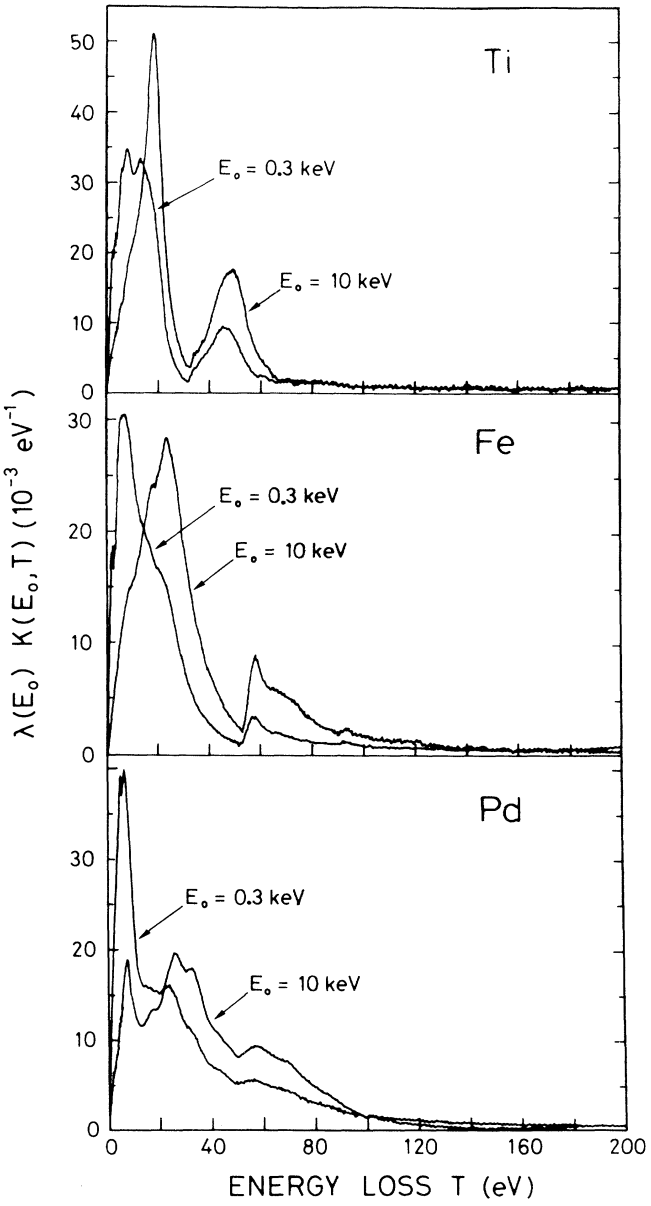

FIG. 7. λ*K* determined from Eq. (3) for Ti, Fe, and Pd for primary electrons of energy 0.3 and 10 keV. Note that the cross section goes smoothly to ~ zero for energy loss exceeding 100 eV without the use of any scaling parameter.

B. Experimentally determined cross sections and comparison to theory

REELS spectra were recorded for Si, Ti, Fe, and Pd for primary energies 0.3 keV $\leq E_0 \leq$ 10 keV and loss energies $0 \leq T \leq 200$ eV while for Cu, Ag, and Au the energy range was restricted to $E_0 \leq 2$ keV and $0 \leq T \leq 100$ eV.

As an example, Fig. 6 shows REELS of Fe, recorded at 0.3- and 10-keV primary electron energy, respectively. Note the huge background of multiply inelastically scattered electrons.

Now, Eq. (3) was applied to these and other spectra and $\lambda(E_0)K(E_0,T)$ determined as shown in Figs. 7–14. In all cases, the cross section goes to zero at high-energy loss as seen in Fig. 7. Note that this is obtained without the use of any fitting parameters, but is a consequence of the ability of the applied formula, Eq. (3), to correctly describe the effects of multiple-scattering events.

At lower energy loss, structure is observed. Thus, e.g., in the case of Fe, excitations at ~55- and 92-eV energy loss are observed. These correspond to the excitation of $3p$ and $3s$ core electrons, respectively. In the energy-loss range below 50 eV characteristic structure is observed which corresponds to interband and plasmon excitations of weakly bound electrons.

As the primary energy is lowered, the relative intensity of the various structures changes. The overall absolute intensity only varies a little with the primary energy. As was pointed out previously,[21] this is to be expected since $\lambda(E_0)\int K(E_0,T)dT=1$. Therefore the product $\lambda(E_0)K(E_0,T)$ is a weak function of E_0. After division by $\lambda(E_0)$, which increases with E_0,[12,13] the resulting cross sections will decrease with E_0 as expected.

For Si, a bulk-plasmon peak is observed at $T_B \simeq 18$ eV

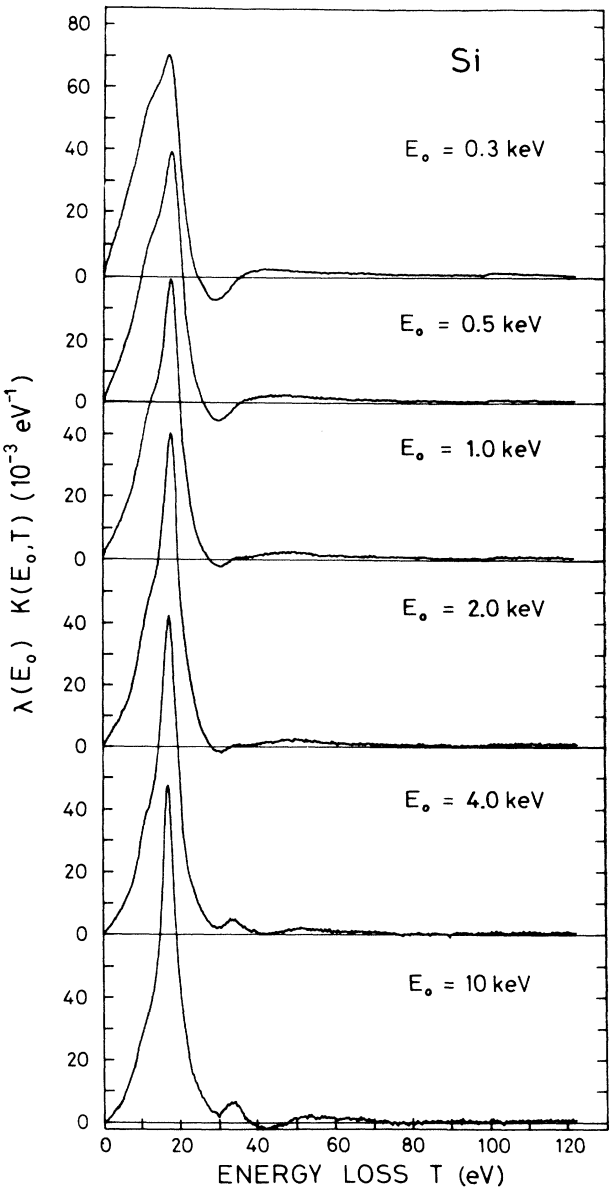

FIG. 8. λK for Si determined from measured REELS and Eq. (3).

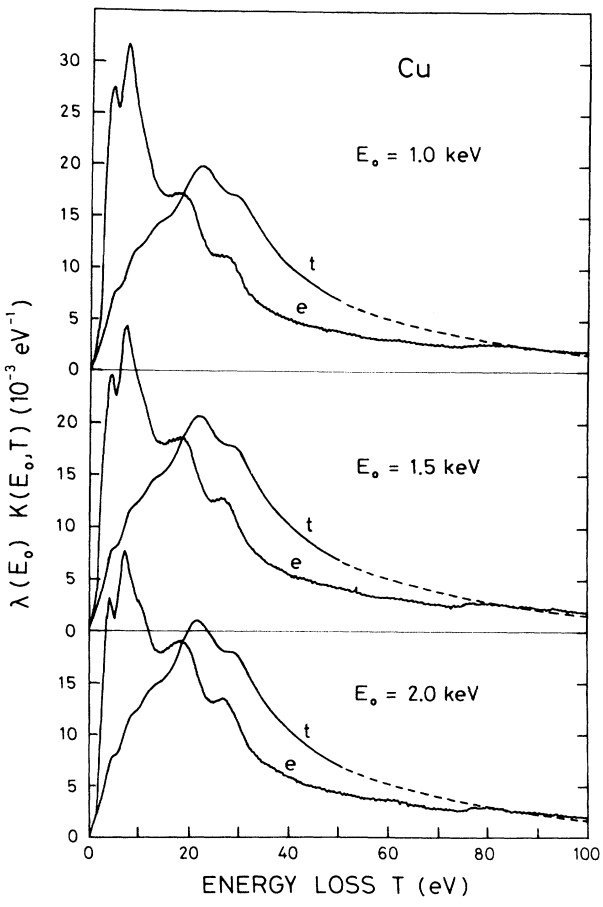

FIG. 9. Curves e, λK for Cu determined from the measured REELS and Eq. (3). Curves t, theoretical λK curves determined from Eq. (4).

and a shoulder corresponding to surface-plasmon excitations at $T_s \simeq 12$ eV. The slight negative cross sections for $T \simeq T_s + T_B \simeq 30$ eV are ascribed to the fact that $K(T)$ varies with depth due to a change with depth in the relative surface- and bulk-plasmon excitation probabilities. Equation (3) is, however, strictly valid only when $K(T)$ is independent of depth. This effect was discussed in detail previously[14] where a similar behavior was observed for aluminum.

The theoretical cross sections determined in the preceding section must be multiplied by $\lambda(E_0)$ to compare with the experimentally determined $\lambda(E_0)K(E_0,T)$ functions. λ has been studied experimentally[12] and theoretically.[13] There are, however, still large differences between the values determined by various approaches. For this reason, λ was here determined by the requirement that the areas of the two sets of cross sections should be identical when integrating over T in the 0–30-eV, 0–50-eV, or 0–100-eV energy range depending on the available range of data for $\mathrm{Im}[-1/\epsilon(0,\omega)]$ (see Sec. IV A). The thus determined values of $\lambda(E_0)$ are listed in Table II. Note that for Ti and Ag, where the interval for normalizing the two areas is 0–100 eV, the determined factors are probably a reasonable approximation for the inelastic mean free path λ. For all the other materials, where the energy interval is 0–30 eV and 0–50 eV, the factors are not believed to be a good measure for λ. It is interesting to note that for Ti and Ag, the λ values determined in Table II for all the energies considered deviate by only 5–10 % from values determined by a recent general formula due to Tanuma, Powell, and Penn.[22] For the

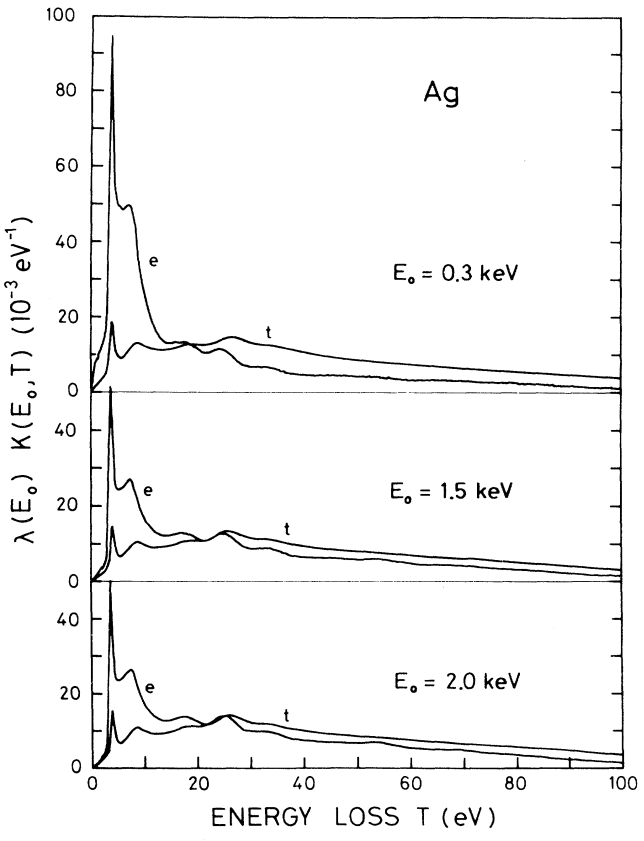

FIG. 10. Curves e, λK for Ag determined from the measured REELS and Eq. (3). Curves t, theoretical λK curves determined from Eq. (4).

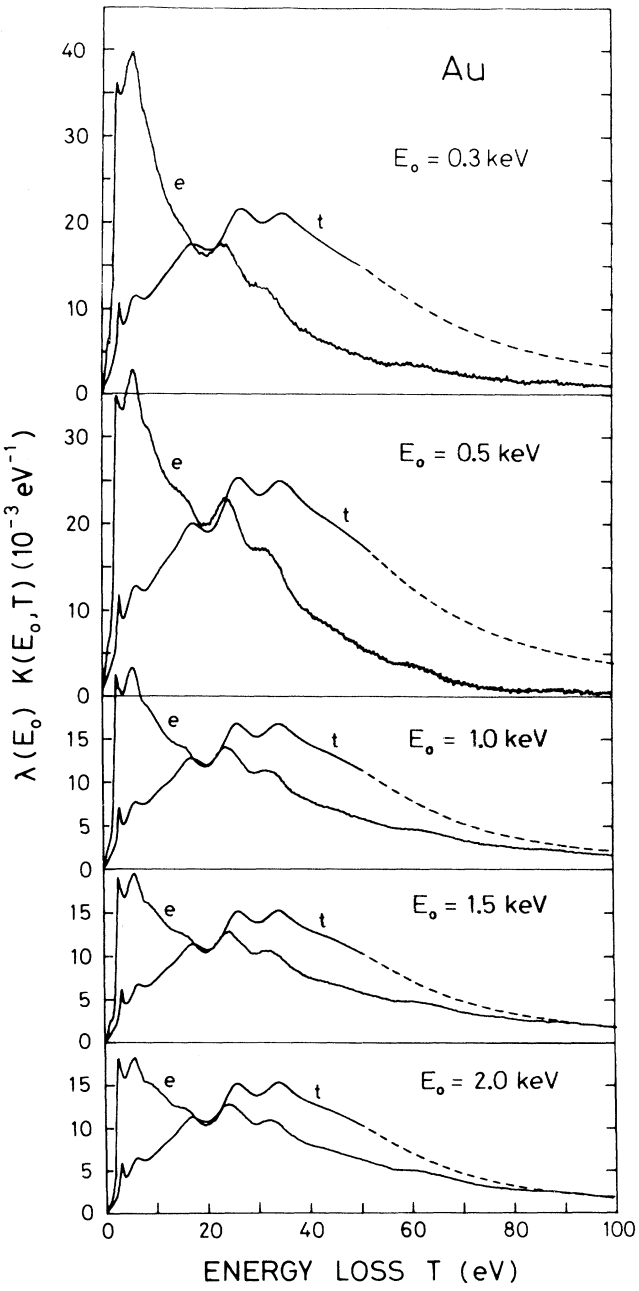

FIG. 11. Curves e, λK for Au determined from the measured REELS and Eq. (3). Curves t, theoretical λK curves determined from Eq. (4).

other materials in Table II, the deviations from this formula are much larger.

The resulting theoretical curves, marked t, are also shown in Figs. 9–14. Note that the theoretical curves have been extended beyond the range of energy loss where the fit of $\mathrm{Im}(-1/\epsilon)$ was made (see Sec. IV A). For Fe, at $E_0=10$ keV (Fig. 13) the agreement with experiment is quite good. As E_0 is lowered, deviations occur. But even at $E_0=3$ keV the comparison is rather good. At still lower energies a peak builds up at ~5–10-eV energy loss at the expense of the broad structure at 15–30 eV. The trend for Pd (Fig. 14) is quite similar. Note here the gradual shift of the peak at $T\cong 27$ eV. This shift is not modeled by theory.

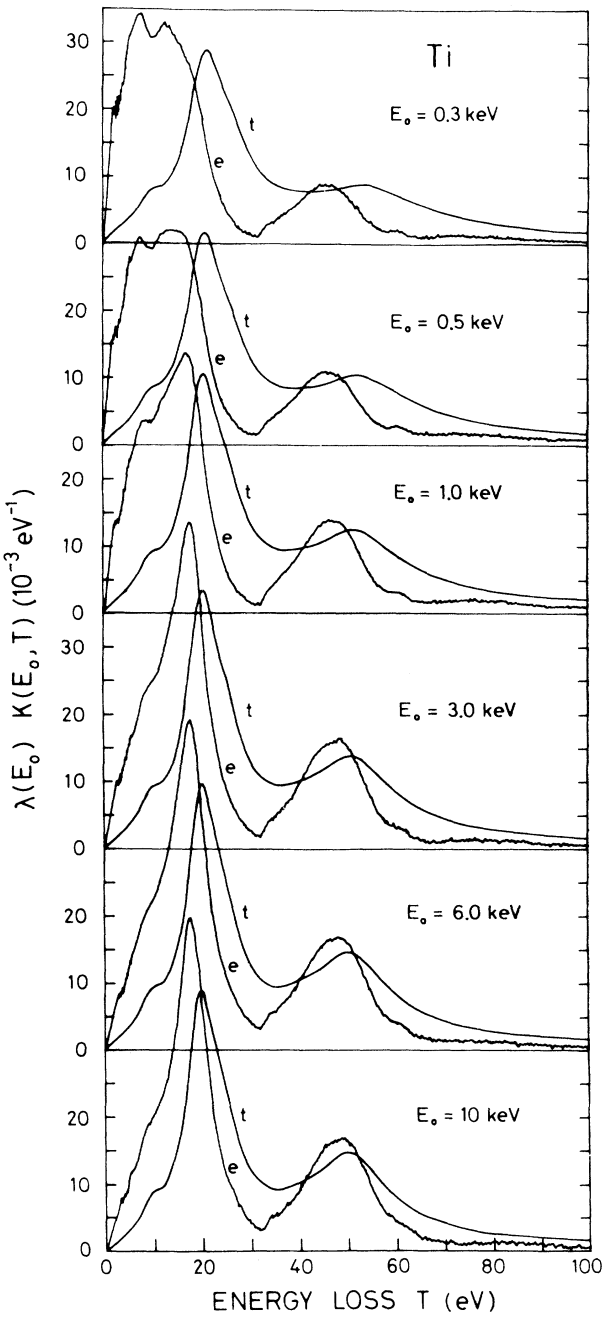

FIG. 12. Curves e, λK for Ti determined from the measured REELS and Eq. (3). Curves t, theoretical λK curves determined from Eq. (4).

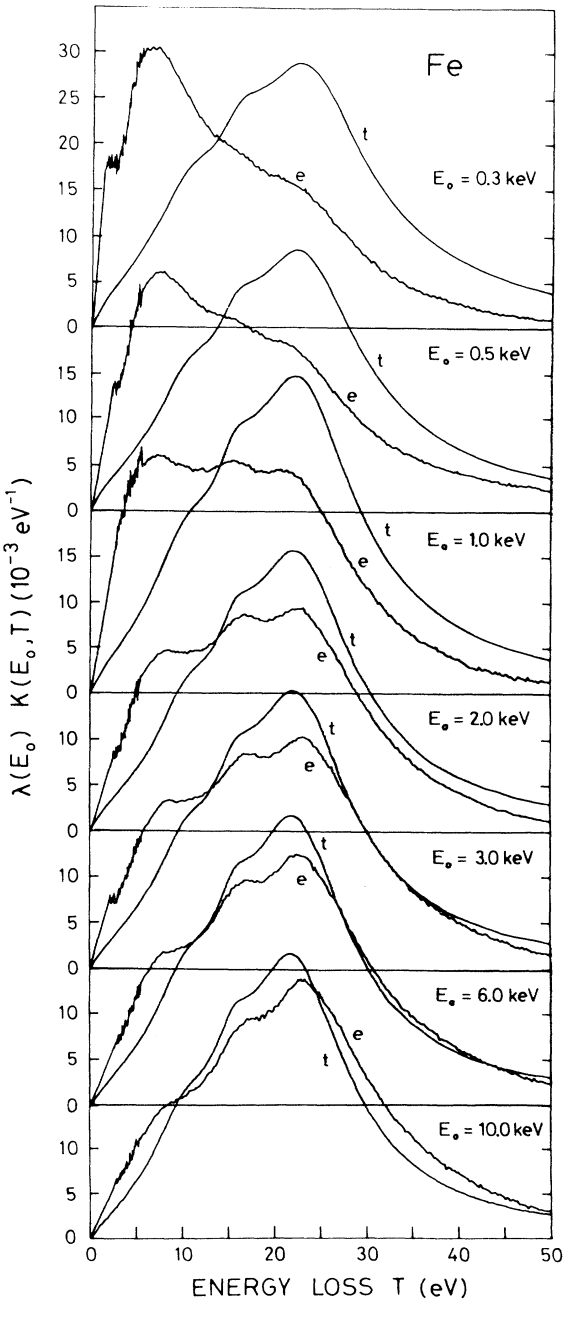

FIG. 13. Curves e, λK for Fe determined from the measured REELS and Eq. (3). Curves t, theoretical λK curves determined from Eq. (4).

For Ti (Fig. 12) the theoretical cross sections deviate more from experiment. Although the difference between theory and experiment is relatively smaller at higher primary energy, the peak positions are shifted even at $E_0=10$ keV. This shift increases at the lower energies and a new peak at $T\sim 8$ eV appears. For Cu, Ag, and Au (Figs. 9–11) the general trend is similar, with a low-energy peak at $T\cong 5-10$ eV gradually increasing in intensity for $E_0\leq 2$ keV.

The observed deviations between theory and experiment could be due to mainly three factors. Firstly, the major assumption for the validity of Eq. (3) is that the medium has uniform scattering properties. This is not strictly true.[5,14] Thus the probability for surface excitations is higher when the electron is near the surface region of the sample and the relative importance of surface excitations is expected to increase with decreasing E_0. To investigate this possible explanation for the peak at ~ 10 eV, we have, on the basis of the complex dielectric function, evaluated the surface loss function $\mathrm{Im}[-1/(\epsilon+1)]$. This function is plotted in Fig. 15 for Fe and Pd, respectively. No new distinct structure appears. However, the intensity in the 5–10-eV relative to the 15–30-eV energy-loss range is higher for $\mathrm{Im}[-1/(\epsilon+1)]$ than for $\mathrm{Im}(-1/\epsilon)$. Thus the observed change in the experimentally determined $K(E_0,T)$ for $T=5-10$ eV at the expense of the 15–30-eV loss range could be due to the excitation of surface plasmons.

Secondly, it is quite conceivable that the simple model assumed in $\mathrm{Im}[-1/\epsilon(k,\omega)]$ for momentum transfers [Eq. (5)] is insufficient. A different k dependence could

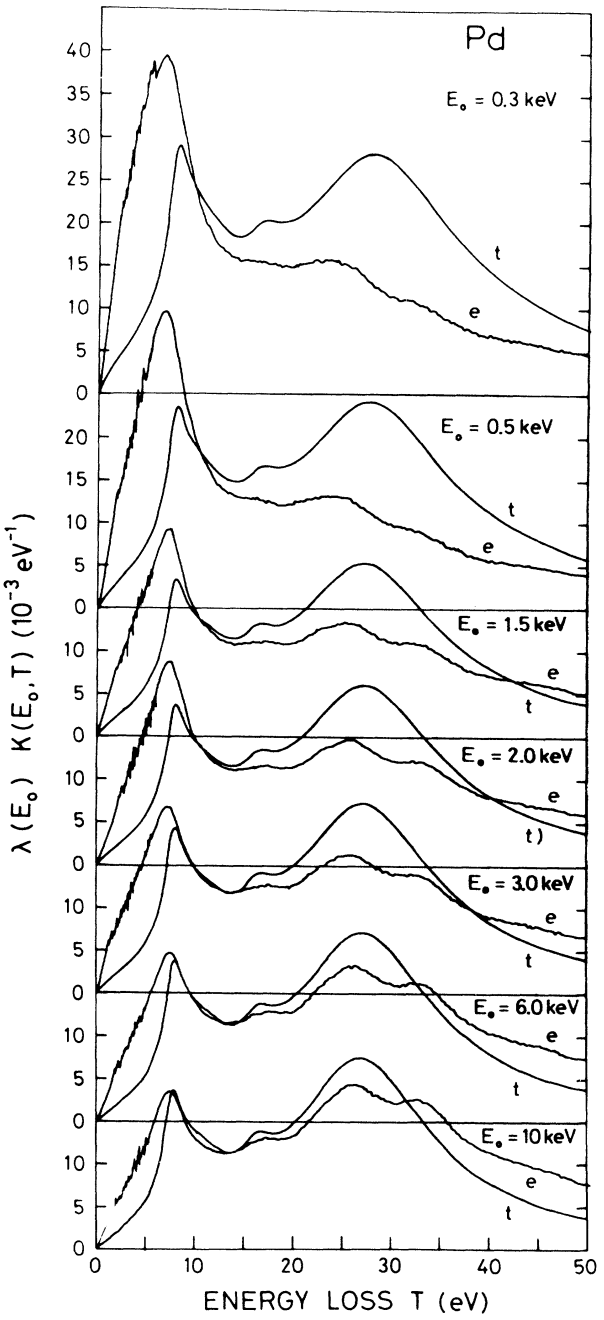

FIG. 14. Curves e, λK for Pd determined from the measured REELS and Eq. (3). Curves t, theoretical λK curves determined from Eq. (4).

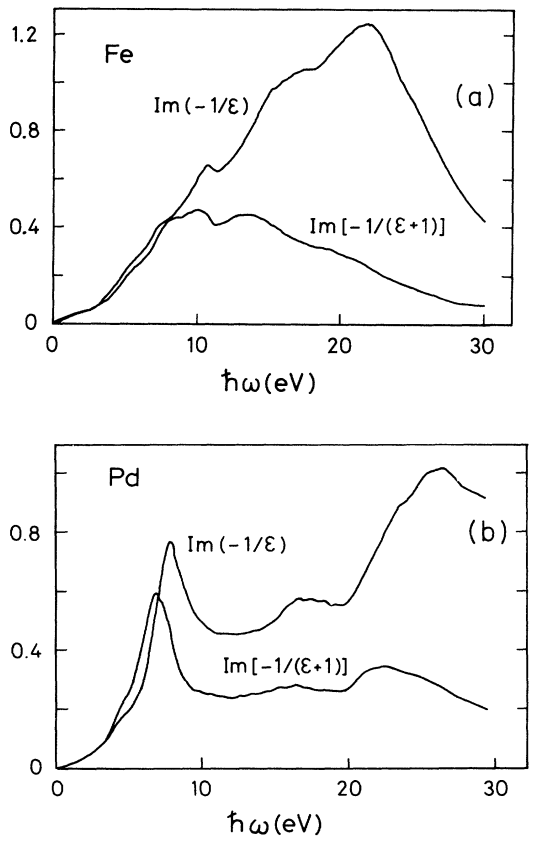

FIG. 15. Bulk and surface loss function evaluated from the data in Ref. 18.

lead both to a shift in the position of peaks as well as to a change in relative peak intensities with primary energy E_0. To make a quantitative analysis of these factors one would need a detailed model for the description of surface-plasmon excitations in the reflection mode as well as improved model dielectric functions.[23–27] It is hoped that the present data will encourage further theoretical work in the future.

Finally, it has been pointed out that the angular deflection in an inelastic-scattering event will, for low-energy electrons scattering on single crystals, cause the effective solid angle to vary with energy loss. This could cause problems for an analyzer like the one used here with a small detection angle.[28] For single crystals the periodic structure of the crystal will focus the electron beam in certain directions and the effect will be large. For polycrystalline solids, elastic scattering is, however, found to be well described by atomic cross sections,[29] which are rather smooth functions of scattering angle. For polycrystalline solids, elastic scattering therefore apparently defocuses the electron beam and the above effects can be neglected in the present investigations.

V. CONCLUSIONS

Reflection electron-energy-loss spectra, analyzed by a recent formula, were applied to investigate inelastic-scattering cross sections of 300–10 000-eV electrons in Si, Ti, Fe, and Pd and of 300–2000-eV electrons in Cu, Ag, and Au. For comparison, theoretical cross sections were evaluated from Drude-Lindhard model dielectric functions. Theory was found to be good at high energies but at low energies deviations from the experiment were observed.

[1]See, for example, H. Raether, *Excitations of Plasmons and Interband Transitions by Electrons,* Vol. 88 of *Springer Tracts in Modern Physics* (Springer, New York, 1980).

[2]M. Inokuti, Rev. Mod. Phys. **43**, 297 (1971).

[3]International Commission on Radiation Units and Measurements, Report No. 37 ISBN 0-913394-31-9, 1984 (unpublished).

[4]*Practical Surface Analysis,* edited by D. Briggs and M. P. Seah (Wiley, New York, 1990), Vol. 1.

[5]S. Tougaard, Surf. Interf. Anal. **11**, 453 (1988).

[6]S. Tougaard, J. Vac. Sci. Technol. A **8**, 2197 (1990).

[7]J. Lindhard, K. Dan. Vidensk. Selsk. Mat.-Fys. Medd. **28**, No. 8 (1954).

[8]R. H. Ritchie and A. Howie, Philos. Mag. **36**, 463 (1977).

[9]J. C. Ashley, J. J. Cowan, R. H. Ritchie, V. E. Anderson, and J. Holzl, Thin Solid Films **60**, 361 (1979).

[10]C. J. Tung and R. H. Ritchie, Phys. Rev. B **16**, 4302 (1977).

[11]S. Tougaard and B. Jørgensen, Surf. Sci. **143**, 482 (1984).

[12]M. P. Seah and W. A. Dench, Surf. Interf. Anal. **1**, 2 (1979).

[13]S. Tanuma, C. J. Powell, and D. R. Penn, Surf. Interf. Anal. **11**, 577 (1988).

[14]S. Tougaard and I. Chorkendorff, Phys. Rev. B **35**, 6570 (1987).

[15]A. Tofterup, Phys. Rev. B **32**, 2808 (1985).

[16]M. P. Seah, Surf. Interface Anal. **2**, 222 (1980).

[17]S. Tougaard, in *Radiation Research,* edited by E. M. Fielden, J. F. Fowler, J. H. Hendry, and D. Scott (Taylor and Francis, London, 1987), Vol. 2, p. 266.

[18]J. H. Weaver, C. Krafka, D. W. Lynch, and E. E. Koch, *Physics Data, Optical Properties of Metals* (Fachinformationszentrum Energie, Physik, Matematik G.m.b.H., Karlsruhe, 1981), No. 18 (ISSN 0344-8401).

[19]C. Wehenkel and B. Gauthé, Phys. Status Solidi B **64**, 515 (1974).

[20]C. Wehenkel, J. Phys. (Paris) **36**, 199 (1975).

[21]S. Tougaard, Solid State Commun. **61**, 547 (1987).

[22]S. Tanuma, C. J. Powell, and D. R. Penn, J. Vac. Sci. Technol. A **8**, 2213 (1990).

[23]R. H. Ritchie, Phys. Rev. **106**, 874 (1957).

[24]E. Colavita, M. De Crescenzi, L. Papagno, R. Scarmozzino, L. S. Caputi, R. Rosei, and E. Tosatti, Phys. Rev. B **25**, 2490 (1982).

[25]G. Chiarello, E. Colavita, M. De Crescenzi, and S. Nanarone, Phys. Rev. B **29**, 4878 (1984).

[26]V. E. Henrich, G. Dresselhaus, and H. J. Zeiger, Phys. Rev. B **22**, 4764 (1980).

[27]Y. Ohno, Phys. Rev. B **39**, 8209 (1989).

[28]J. A. D. Matthew, E. Bertel, and F. P. Netzer, Surf. Sci. **184**, L389 (1987).

[29]A. Jablonski, J. Gryko, J. Kraaer, and S. Tougaard, Phys. Rev. B **39**, 61 (1989).